Investigation of the nanocomposite material $YBa_2Cu_3O_{7-\delta}$ + ZrO_2 as a resistive superconducting fault-current limiter.

A.V. Ushakov[1,2], I.V. Karpov[1,2], V.G. Demin[1,2], A.A. Shaihadinov[1,2], A.I. Demchenko[2], L.Yu. Fedorov[1,2*], E.P. Bachurina[1,2], E.A. Goncharova[2]

[1] Federal Research Center Krasnoyarsk Scientific Center of the Siberian Branch of the Russian Academy of Science, 660036, Krasnoyarsk, Russia

[2] Siberian Federal University, Krasnoyarsk, 660041, Russia

* Author to whom correspondence should be addressed. Electronic mail: 1401-87@mail.ru

Abstract. The effects of nanoscale inclusions ZrO_2 as the second component of the composites on the magnetic and transport properties of superconducting polycrystals $YBa_2Cu_3O_{7-\delta}$ are studied. Samples of $YBa_2Cu_3O_{7-\delta}$ with different (0.5, 4, 8 и 12 wt.%) contents of ZrO_2 nanoparticles were synthesized. Measurements of the magnetization in the field range up to 5 T and recalculation using the Bean model showed that JC in the case of composite samples is larger than the initial one in the entire range of the magnetic field. The results of experimental studies of switching superconducting fault-current limiter in AC voltage networks based on high-temperature superconductors (HTSC) of the 2nd generation are given. The stand contains a series-connected HTSC module and a high-speed current switch with a shutdown time of 9 ms. The high efficiency of samples from the nanocomposite material $YBa_2Cu_3O_{7-\delta}$ + ZrO_2 as a resistive superconducting fault-current limiter was shown.

Keywords: YBCO ceramics, critical current, resistive superconducting fault-current limiter.

Introduction. One of the promising ways of limiting fault currents (FC) could be the creation of current-limiting devices based on high-temperature superconductors (HTSC) of the 2nd generation [1]. Such materials, in comparison with previous-generation superconductors, are characterized by reduced metal content (small thickness of the substrate and stabilizer), additional heat removal, a higher critical current value and a high resistance to emergency currents in a normal state. In normal operation, the device has practically no influence on the mode of the system, while in emergency operation, it introduces the resistance, necessary to limit the fault current to the required level, into the network.

Based on design features, two basic concepts of a superconducting fault current limiter (SFCL) can be distinguished: resistive and inductive. Other schematic solutions are based on

these concepts [2]. In the case of inductive design, the magnetic coupling between the superconducting element and the winding is carried out through a three-core magnetic conductor [3]. For example, the ABB company developed three-phase current limiter (1.2 MVA) with a cylindrical screen consisting of 16 rings which were made from the superconducting ceramics Bi-2212, which was tested and operated during the year [4]. The operation of an inductive current limiter is concerned with the presence of magnetic stray fields, which can adversely affect the use of a metal cryostat and increase power loss.

The resistive design of a SFCL is based on the nonlinearity of the superconductor resistance and it could use massive elements or coils [5]. When superconducting coils are used as superconducting elements, they are arranged in such a way to make the total inductance of the limiter possibly minimal [6]. A resistive superconducting current limiter contains a HTSC module placed in a cryostat with liquid or supercooled nitrogen, acting as a cooling agent, and high-voltage current inputs of a special design. The basic disadvantage of a resistive SFCL is considerable heat generation, the presence of magnetic stray fields, overheating during a short circuit, and a relatively long response time.

The paper [7] describes the development of composite material based on the $YBa_2Cu_3O_{7-\delta}$ granular superconductor and CuO electric arc nanopowders [8–12]. The addition of CuO nanopowders improves the quality of the sintered composites, with significant increase in the critical current density, as well as a peak effect in the region of strong magnetic fields [13]. Changing the concentration of CuO nanopowders make it possible to achieve a smooth regulation of the critical current density and a decrease in the transition time to the normal state. At the same time, there is evidence [14, 15] that ZrO_2 in the HTSC / nano ZrO_2 composite leads to an impressive increase in the critical current and to a smaller attenuation of the magnetic field.

This paper presents the results of measuring the magnetic and transport characteristics of the obtained nanocomposite material $YBa_2Cu_3O_{7-\delta}$ + ZrO_2, parameters of a polycrystalline (ceramic) HTSC device connected in accordance with the series subcircuit in the current limiting mode to 1200 A during the first half-wave of an alternating current. Theoretically, such a ballast resistance at a transport current less than the critical (J_c) is equal to zero and, when an emergency situation occurs, accompanied by an increase in current above J_c, it “switches on” into the circuit and limits the current to a given value. In the practical implementation of such a limiter, it is necessary to overcome a number of technical challenges, among them are the problem of contacts in HTSC, the problem of heat removal from the HTSC protection element in the short circuit protection mode (when the HTSC

remains the only consumer) and the resulting task of negotiating the HTSC element according to the voltage drop in the resistive state with the voltage of the protected circuit, which determines its geometrical dimensions and the power developed in a unit of volume.

Experimental. The samples for measurements were made by pressing and sintering (temp. 930 °C) the prepared HTSC powder $YBa_2Cu_3O_{7-\delta}$ with ZrO_2 nanoparticles coated on the surface. The preparation of composites $Y_1Ba_2Cu_3O_{7-\delta} + xZrO_2$ was carried out on a device described in detail in paper [16]. A distinctive feature was the use as a cathode for spraying zirconium of technical purity. The remaining parameters are further described in paper [15]. During the experiment, the samples with 0.5, 4, 8 и 12 wt.% ZrO_2 were used. The samples were protected on the top with a layer of silver with a thickness of about 2 microns without a stabilizing copper shell, which is better suited for use in resistive superconducting current limiters, since they have the highest resistance in a normal non-superconducting state. The typical sample size was 2×7×44 mm. To increase the area to the maximum possible, the current contacts were covered with In – Ga eutectic. The assembled unit was placed in a bath with liquid nitrogen. The studies were conducted on a low-voltage testing equipment, which contained a transformer with an output voltage U_0 = 20 V (rms value), a network key K_1 with an electromagnetic drive, a load resistance R_0 = 0.2 Ω, and a control system (Fig. 1). A chain with the connected in series thyristor key *VT* and the additional resistance R_1 was wired parallel to the R_0 resistance. The key *VT* was used to simulate the occurrence of fault current, the amplitude of which was regulated by changing the resistance R_1. The test samples R_{HTSC} and switch K_2 were connected to the output of the transformer before the load resistance R_0. During the experiments, the HTSC samples were immersed in a Dewar vessel filled with liquid nitrogen.

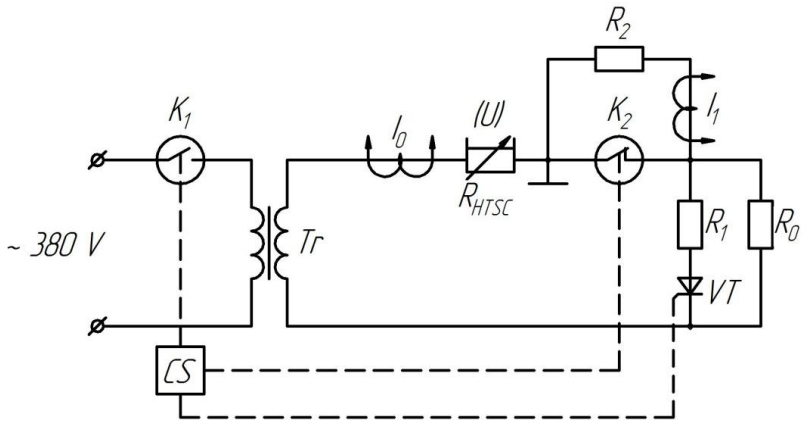

Figure 1. Electrical circuit of the testing equipment (K_1 – network key, *VT* – load generation key, K_2 –turn-off key, CS – control system, R_0 – load resistance, R_1 – additional resistance, R_2 – shunt resistance)

The control system (CS) generated signals with an adjustable turn-on delay K_1 at the moment of circuit voltage maximum, turn-on *VT* to generate a fault current approximately one period after the start of the load current flow, and turn-off K_2 at the end of the first half-wave of the current. The expected amplitude of the first half-wave of the fault current was 4700 A.

To study the recovery mode of the superconducting element of the HTSC after the current was turned off by the K_2 switch, it was shunted by resistance R_2. The total duration of current flow in the HTSC element was about 300 ms.

The inherent resistance of the low-voltage network in the fault mode was lower (less than 15 mOhm) compared with the resistance of HTSC elements after the transition to the normal state. Therefore, almost all the circuit voltage was applied to HTSC. Such conditions are close to the actual conditions of current limitation in AC networks with a given voltage. The change in the parameters of the current limitation was regulated by changing the additives of ZrO_2 nanodispersed powder.

For each sample, oscillographic testing of current and voltage was performed. The limited current i_{lim} was measured by a galvanically isolated sensor with a sensitivity of 2560 A/V The electrical signals were recorded using P6139A testers on a Tektronix DPO 4034 oscillograph, and then they were saved and processed on a personal computer. While being processed on a computer, the inductive component of the voltage drop on the HTSC element was subtracted from the measurement data.

The magnetic measurements were carried out with the MPMS-XL5 unit. Debye X-ray patterns were recorded on the D8 ADVANCE diffractometer (Bruker AXS) in CuKα monochromatic radiation. The measurements of the isothermal dependences of the magnetization on the magnetic field were carried out at a temperature of 77 K. The critical current density of the samples was estimated from the magnetic hysteresis loop using the extended critical state model [17].

Results. Figure 2a shows the diffraction patterns of the obtained $YBa_2Cu_3O_{7-\delta} + xZrO_2$ composites (x = 0.5, 4, 8, and 12 wt.%) at room temperature. An analysis of the diffraction pattern showed that all samples crystallize in the orthorhombic phase with the space group Pmmm. The lattice parameters and other set parameters of all samples are listed in Table 1. All structural parameters, such as lattice parameters, orthorhombicity, unit cell volume, remain unchanged.

The presence of ZrO_2 in the YBCO matrix is evident due to the appearance of additional peaks in the diffraction pattern, the intensity of which increases with increasing ZrO_2

concentration in YBCO. Monoclinic (2Θ = 28.20, 31.20, 35, *hkl*: (-111), (111), (002)) and tetragonal (2Θ = 30.02, 49.8, *hkl*: (101), (112)) ZrO_2 phase nanoparticles. Since the transport properties strongly depend on the characteristic features of the microstructure, it becomes important to investigate the effect of adding ZrO_2 on the microstructure of YBCO. Figure 2b and 2c shows the SEM micrograph of the obtained $YBa_2Cu_3O_{7-\delta}$ + $xZrO_2$ composite. The nanopowder is evenly distributed over the surface of YBCO particles and, moreover, it fills the intergranular space and pores, which can act as a catalyst for improving the quality of the structure at the grain boundaries [18]. This forces the grain to behave in a consistent manner and introduces significant changes in mechanical and transport measurements. This observation is consistent with measurements of magnetization.

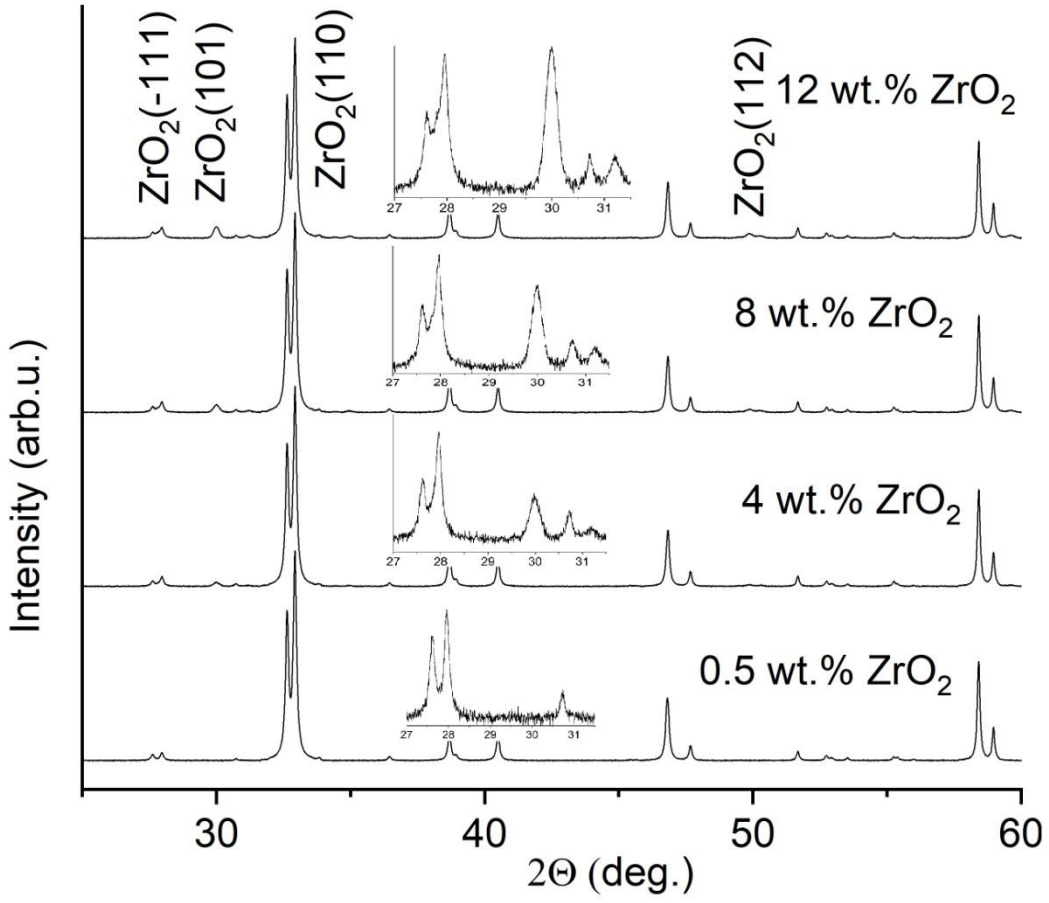

Figure 2a. Diffraction patterns of the composites obtained $YBa_2Cu_3O_{7-\delta}$ + $xZrO_2$ (x = 0.5, 4, 8, 12 wt.%)

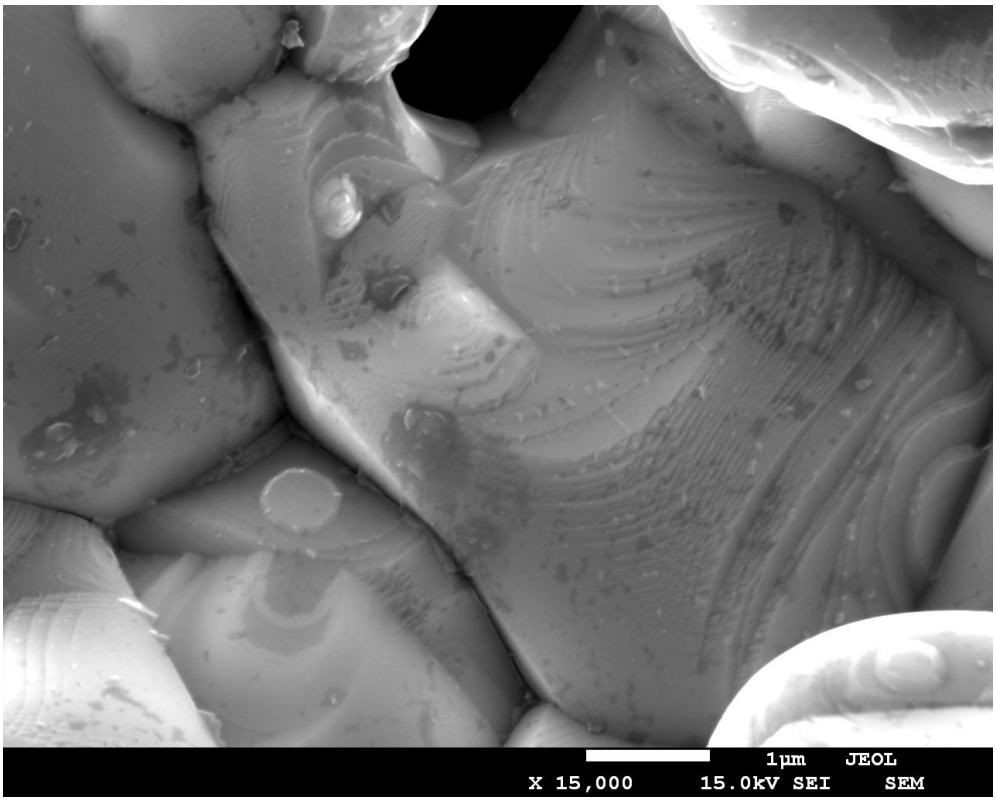

Figure 2b. SEM photomicrograph of the obtained composite $YBa_2Cu_3O_{7-\delta}$ + 0.5 wt.% ZrO_2

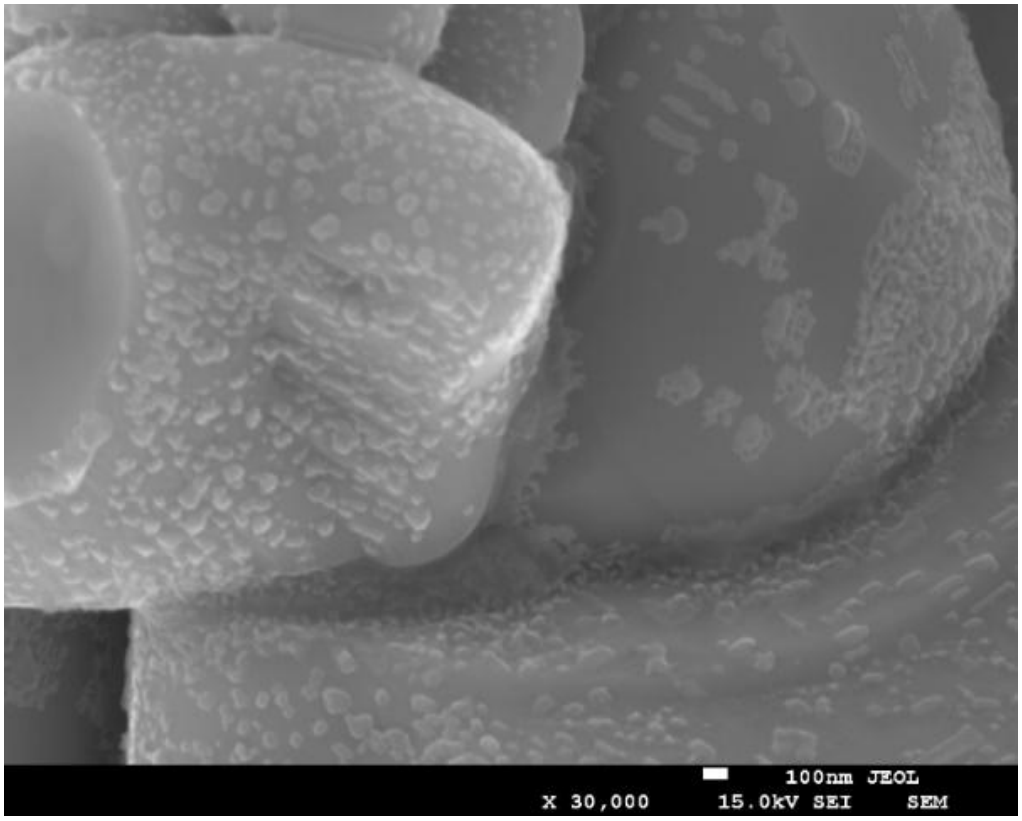

Figure 2c. SEM photomicrograph of the obtained composite $YBa_2Cu_3O_{7-\delta}$ + 12 wt.% ZrO_2

Table 1. The lattice parameters and the volume of the YBCO cell in the composite.

Sample	*a*(Å)	*b*(Å)	*c*(Å)	Vol.(Å^3)
YBCO	3.825	3.888	11.695	173.923
YBCO+0.5 wt.% ZrO_2	3.828	3.890	11.688	174.045
YBCO+4 wt.% ZrO_2	3.827	3.889	11.687	173.940
YBCO+8 wt.% ZrO_2	3.828	3.889	11.689	174.015
YBCO+12 wt. % ZrO_2	3.827	3.885	11.681	173.672

On SEM micrographs, it is also seen that ZrO_2 does not react with YBCO to form a new phase, but remains as an adhesive material at the grain boundaries, thus making YBCO more attractive for technological applications. Additionally, X-ray phase analysis did not reveal the presence of products of interaction of ZrO_2 nanoparticles with the HTSC matrix. To study the effect of ZrO_2 on the temperature of the superconducting transition (T_c) YBCO, the change in electrical resistivity as a function of temperature was studied. The data are normalized per unit at 300 K, and the change in the normalized specific resistance of composite samples with temperature is shown in Figure 3. All samples show a superconducting transition of about 90 K, but the transition broadening is greater in the case of composite samples than the original ones. This suggests that the broadening of the transition is apparently due to an increase in the concentration of nano-ZrO_2 in the YBCO matrix. The superconducting transition temperature T_c practically did not change with the addition of ZrO_2 in YBCO. This is an important result, since there are examples in the literature when the introduction of the secondary phase leads to an undesirable decrease in the transition temperature [19]. Although ZrO_2 is a dielectric material, the resistivity of the normal state (electrical resistivity of composite $YBa_2Cu_3O_{7-\delta}$ + $x ZrO_2$ at 300 K ρ=1150±20 μΩ·cm) does not increase with the addition of ZrO_2, as one would expect.

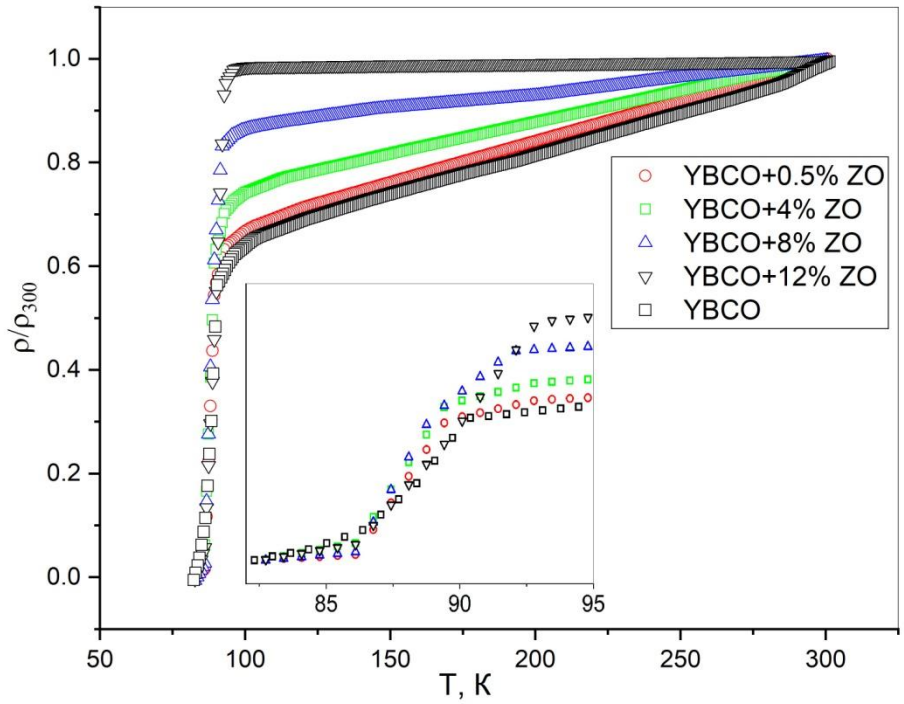

Figure 3. Temperature-dependent normalized resistivity, ρ/ρ_{300} composites $YBa_2Cu_3O_{7-\delta} + xZrO_2$ (x = 0.5, 4, 8, 12 wt.%).

The critical current density strongly depends on the boundary region of the grains and the nature of the cohesion of the grains in J_C is expected. In order to establish and quantify the change in J_C, isothermal magnetization measurements were made, and these results are shown in Figure 4a. The measurements were carried out in a wide magnetic field range up to 5T and at a temperature of 5K, where it is assumed that there is no flux creep. The applied magnetic field is set parallel to the long axis of the measured sample, which ensures maximum area and helps to avoid demagnetization. Obviously, as the field increases from 0 to H_{C1}, the corresponding magnetization also increases in the opposite direction in accordance with the Meissner effect.

As soon as the applied field exceeds H_{C1}, the magnetic flux begins to penetrate into the sample, leading to the formation of Abrikosov vortices. The density of the magnetic flux lines (normal nuclei) is determined by the equilibrium between the decrease in free energy and mutual repulsion between the vortices. In an increasing magnetic field, normal nuclei are packaged closer to each other, so the average flux density increases in the material, and the magnetization decreases. It was found that the decrease in magnetization is less in the case of a composite sample compared to the original sample [20]. The magnetic flux lines in the mixed state of any superconductor can be fixed by various interactions, such as impurities,

residual stresses, point defects, expanded defects and secondary phases, etc. Thus, the introduction of ZrO_2 as a secondary phase in YBCO leads to pinning lines magnetic flux, which leads to a smaller decrease in magnetization compared to the original outside of H_{C1}. In addition, pinning the magnetic flux lines by introducing a secondary phase leads to irreversibility of the magnetization, thereby enhancing J_C. Using the Bean's critical state model [17], the critical current density (J_C) of composite samples is derived from the width of the M-H loop and are presented in Figure 4b.

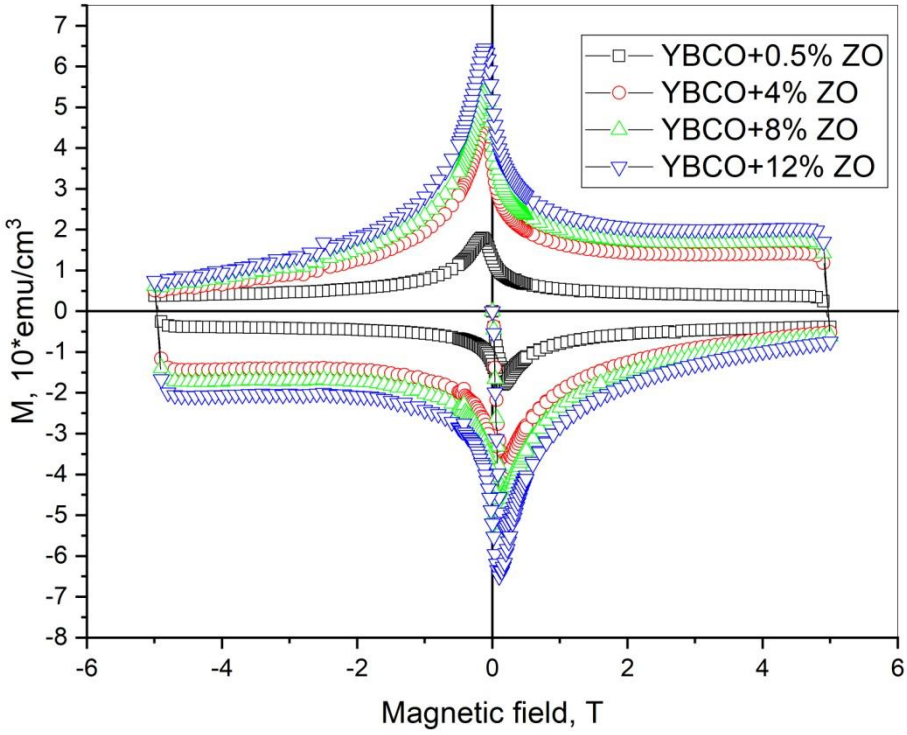

Figure 4*a*. Isothermal hysteresis loops for magnetization of YBCO + $x$$ZrO_2$ samples (x = 0.5, 4, 8, and 12 wt.%) at 5 K

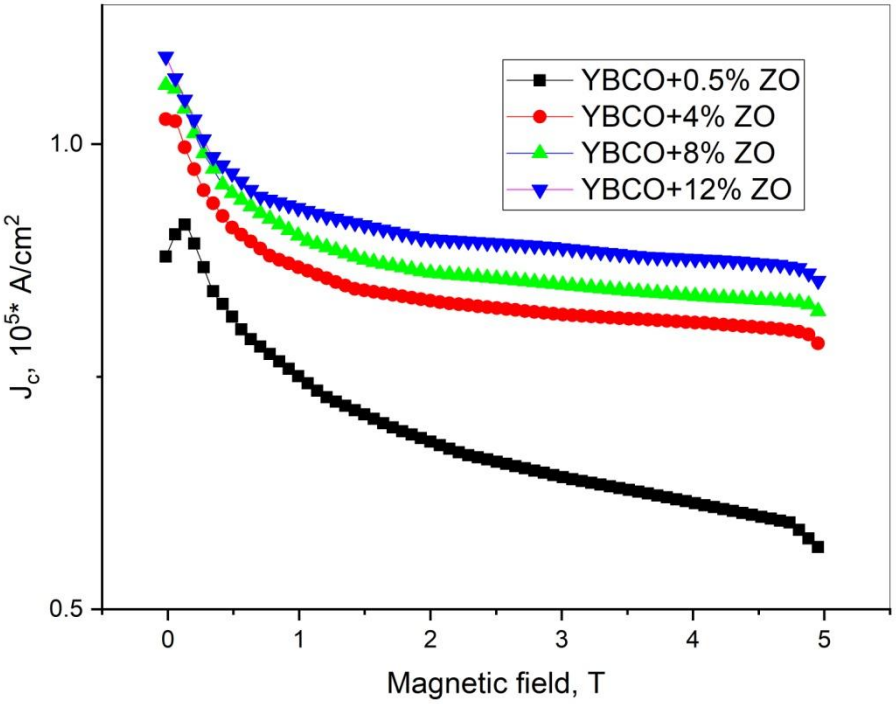

Figure 4*b*. J_C curves depending on the applied magnetic field for samples YBCO + $x$$ZrO_2$ (x = 0.5, 4, 8, and 12 wt.%) at 5 K

The critical current density depending on the applied magnetic field for different composite samples is shown in Figure 4b. It was found that J_C in the case of composite samples is larger than the initial one in the entire range of the magnetic field. The peak J_C value is 6.7×10^4 A/cm^2 for the initial sample and 1.8×10^5 A/cm^2 for YBCO + 8 wt.% ZrO_2. Thus, for a given concentration of ZrO_2, J_C is increased by a factor of 3. In addition, J_C at 50 kOe is almost 10 times more than the original.

The gain of J_C is explained by pinning the magnetic flux of ZrO_2 in YBCO. Zr-doping in YBCO has been studied extensively since the first work by J. L. Macmanus-Driscoll et al [21]. The primary effect of the "Zr" doping is the formation of $BaZrO_3$ nanostructures (nanoparticles, nanorods, etc) that serve as strong pinning centers of magnetic vortices. The most favorable growth of ZrO_2 in YBCO occurs in the form of islands and creates columnar defects in YBCO, which are responsible for increasing the critical current density [13]. The reason for this enhancement of pinning may be due to the fact that ZrO_2, in addition to increasing the binding of grains by filling in cracks and voids, also creates artificial pinning centers that prevent the movement of magnetic flux lines. These artificial pinning centers are responsible for enhancing J_C even at high applied magnetic fields, which makes YBCO interesting for technological applications. One of the most convenient ways to increase J_C

superconducting materials is to create extended defects that act as artificial pinning centers, other than those that occur naturally. The effect of pinning centers is better when their dimensions are of the order of the coherence length. In this case, the most favorable growth of ZrO_2 in YBCO has the appearance of islands and creates columnar defects in YBCO, which are responsible for increasing the critical current density.

The results of studying the produced composites and their application as a resistive current limiter are shown in Figure 5. After the contactor K_1 was turned on, a load current began to flow in the circuit (the first one and a half periods), the amplitude of which (155 A) was about 2 times less than that of the critical current I_c. To demonstrate the effect of limiting the fault current, oscillographic testing of the current was carried out with simulation of fault current appearance without an HTSC element. In this case, a current i_f with an aperiodic component of 4700 A amplitude flowed in the circuit. With HTSC present, the current in the circuit was limited due to a nonlinear increase in the resistance of the superconductor after its transition to the normal (non-superconducting) state. The limiting current I_{max} was determined by the degree of HTSC heating during the current half-wave.

Figure 5a shows the current-limiting mode for the HTSC sample without addition of nano-dispersed ZrO_2 powder at $R_1 = 0$. Figure 5*a* was obtained by superimposing oscillograms of the limiting current i_{lim} and voltage on the HTSC and oscillograms of the fault current I when no HTSC are present in the sample. In this case, the depth of the current limiting was $i_f / i_{\text{lim}} >> 7$.

The oscillograms of current and voltage with different weight additives of nano-dispersed ZrO_2 powder, obtained at $R_1 = 0$, are shown in Figure 5*b*.

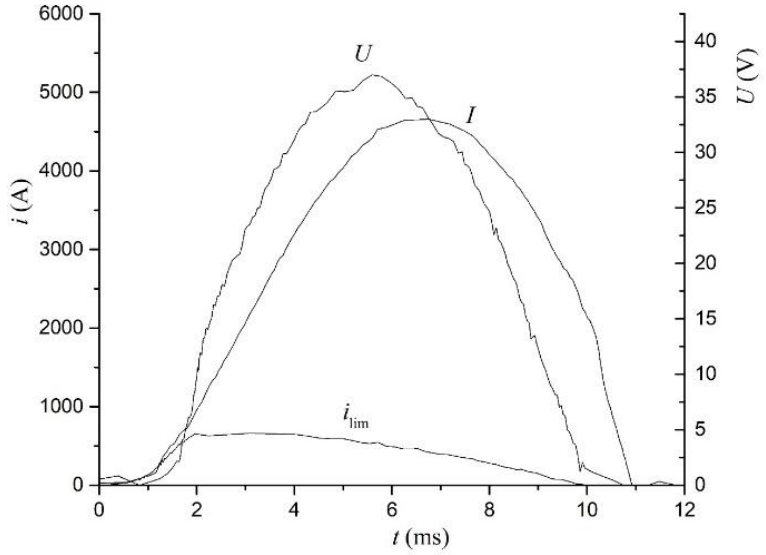

Figure 5*a*. Oscillograms of fault current *I*, limiting current i_{lim} and voltage *U* for a sample of HTSC without addition of nano-dispersed ZrO_2 powder.

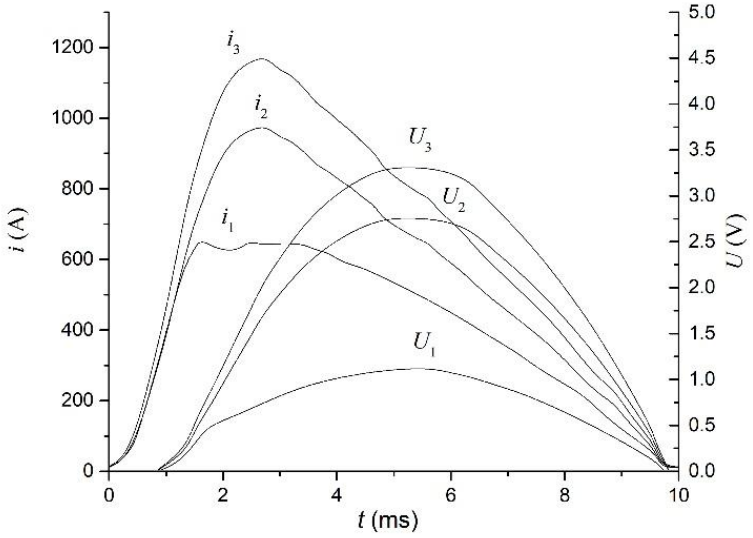

Figure 5*b*. Oscillograms of voltage and current for the sample of HTSC with different content of nano-dispersed powder ZrO_2: 1 – 4 wt.%, 2 – 8 wt.%, 3 – 12 wt. %.

When the content of the nano-dispersed ZrO_2 powder increased, the character of changing the voltage and current on the sample coincided with the critical current calculated from the magnetization loops. Therewith, the delay in the moment of appearing the voltage on the HTSC element increased. A characteristic feature of the change in the current and the voltage over time is the presence of the moment at which a noticeable decrease in the rate of the current and the voltage rise occurred. This moment corresponds to the heating of the HTSC and the beginning of its transition to the normal state. The transition time of the HTSC from the superconducting to the normal state varied depending on the content of the nano-dispersed ZrO_2 powder from 1 ms to 1.5 ms.

Conclusion. Thus, it was found that the addition of nanoscale ZrO_2 particles leads to an increase in the critical current density at T = 77 K for concentrations of 4-12 wt.%. Such an increase in the critical current is associated with ZrO_2 nanoparticles that appear on the surface of superconducting granules. These granules become effective pinning centers for the Abrikosov vortex. As the temperature rises, effective pinning occurs on larger ZrO_2 particles. The performed experiments demonstrated the effectiveness of the proposed approach to the problem of limiting and disconnecting a fault current in AC circuits.

Acknowledgment. The work was performed with a support of the grant of the Russian Science Foundation (project no. 16-19-10054)

References

1. Noe M., Steurer M. High-temperature superconductor fault current limiters: concepts, applications, and development status // Superconductor Science and Technology. 2007. Vol. 20. R15–R29. doi:10.1088/0953-2048/20/3/R01.

2. Paul W., Chen M., Lakner M., Rhyner J., Braun D., Lanz W. Fault current limiter based on high temperature superconductors – different concepts, test results, simulations, applications // Physica C: Superconductivity. 2001. Vol. 354. no.1-4. pp. 27-33. doi: 10.1016/s0921-4534(01)00018-1.

3. Joo M. Reduction of fault current peak in an inductive high-T_c superconducting fault current limiter // Cryogenics. 2005. Vol. 45. no.5. pp. 343-347. doi: 10.1016/j.cryogenics.2004.11.007.

4. Paul W., Chen M., Lakner M., Rhyner J., Widenhorn L., Guérig A. Test of 1.2 MVA high-T_c superconducting fault current limiter // Superconductor Science and Technology. – 1997. Vol.10. no.12. pp. 914-918. doi: 10.1007/978-4-431-66879-4_292.

5. Bock J., Breuer F., Walter H., Elschner S., Kleimaier M., Kreutz R., Noe M. CURL 10: development and field-test of a 10 kV/10 MVA resistive current limiter based on bulk MCP- BSCCO 2212 // IEEE Transactions on Applied Superconductivity. 2005. Vol.15. no.2. pp. 1955-1960. doi: 10.1109/tasc.2005.849344.

6. Elschner S., Breuer F., Noe M., Rettelbach T., Walter H., Bock J. Manufacturing and testing of MCP 2212 bifilar coils for a 10 MVA fault current limiter // IEEE Transactions on Applied Superconductivity. 2003. Vol. 13. no.2. pp. 1980-1983. doi: 10.1109/tasc.2003.812954.

7. Lepeshev A.A., Patrin G.S., Yurkin G.Yu., Vasiliev A.D., Nemtsev I.V., Gokhfeld D.M., Balaev A.D., Demin V.G., Bachurina E.P., Karpov I.V., Ushakov A.V., Fedorov L.Yu., Irtyugo L.A., Petrov M.I. Magnetic properties and critical current of superconducting nanocomposites (1-x)$YBa_2Cu_3O_{7-\delta}$ + xCuO // Journal of Superconductivity and Novel Magnetism. 2018. Vol. 30, No 12, pp. 3351-3354. doi: 10.1007/s10948-018-4676-x.

8. Lepeshev A.A., Ushakov A.V., Karpov I.V., Balaev D.A., Krasikov A.A., Dubrovskiy A.A., Velikanov D.A., Petrov M.I. Particularities of the magnetic state of CuO nanoparticles produced by low-pressure plasma arc discharge // Journal of Superconductivity and Novel Magnetism. 2017. Vol. 30, No 4, pp. 931-936. doi: 10.1007/s10948-016-3885-4.

9. Ushakov A.V., Karpov I.V., Lepeshev A.A., Petrov M.I. Plasma-chemical synthesis of copper oxide nanoparticles in a low-pressure arc discharge // Vacuum. 2016. Vol. 133, pp. 25-30. doi: 10.1016/j.vacuum.2016.08.007.

10. Ushakov A.V., Karpov I.V., Lepeshev A.A. Peculiarities of magnetic behavior of CuO nanoparticles produced by plasma-arc synthesis in a wide temperature range // Journal of Superconductivity and Novel Magnetism. 2017. Vol. 30, No 12, pp. 3351-3354. doi: 10.1007/s10948-017-4311-2.

11. Ushakov A.V., Karpov I.V., Lepeshev A.A., Petrov M.I., Fedorov L.Yu. Specific Features of the Behavior of Electroarc CuO Nanoparticles in a Magnetic Field // Physics of the Solid State. 2015. Vol. 57, No. 5, pp. 919–923. DOI: 10.1134/S1063783415050303.

12. Ushakov A.V., Karpov I.V., Lepeshev A.A., Fedorov L.Yu. Copper Oxide of Plasma-Chemical Synthesis for Doping Superconducting Materials // International Journal of Nanoscience. 2017. Vol. 16, No. 4, p. 1750001. doi: 10.1142/S0219581X17500016.

13. Ushakov A.V., Karpov I.V., Lepeshev A.A., Petrov M.I. Enhancing of magnetic flux pinning in $YBa_2Cu_3O_{7-x}$/CuO granular composites // J. Applied Physics. 2015. Vol. 118, No. 2, p.023907. doi: 10.1063/1.4926549.

14. De Keukeleere K., Cayado P., Meledin A., Vallès F., De Roo J., Rijckaert H., Pollefeyt G., Bruneel E., Palau A., Coll M., Ricart S., Van Tendeloo G., Puig T., Obradors X., Van Driessche I. Superconducting $YBa_2Cu_3O_{7-\delta}$ Nanocomposites Using Preformed ZrO_2 Nanocrystals: Growth Mechanisms and Vortex Pinning Properties // Advanced Electronic Materials. 2016. Vol. 2, p. 1600161. https://doi.org/10.1002/aelm.201600161.

15. Ushakov A.V., Karpov I.V., Lepeshev A.A., Petorv M.I., Fedorov L.Yu. Study of Magnetic Flux Pinning in Granular $YBa_2Cu_3O_{7-y}$/nanoZrO_2 Composites // JETP Letters. 2014. Vol. 99, pp. 99. doi: 10.1134/S002136401402009X.

16. Karpov I.V., Ushakov A.V., Lepeshev A.A., Fedorov L.Yu., Dorozhkina E.A., Karpova O.N., Shaikhadinov A.A., Demin V.G. Device for Increasing the Magnetic Flux Pinning in Granular Nanocomposites Based on the High-Temperature Superconducting Ceramic // Technical Physics. 2018. Vol. 63, No. 2, pp. 230-234. doi: 10.1134/S1063784218020196.

17. Gokhfeld D.M., Balaev D.A., Petrov M.I., Popkov S.I., Shaykhutdinov K.A., Valkov V.V. Magnetization asymmetry of type-II superconductors in high magnetic fields // J. Appl. Phys. 2011. Vol. 109, p. 033904. https://doi.org/10.1063/1.3544038.

18. Orlova T.S., Laval J.Y., Nguyen-van-Huong C., Dubon A. Effect of ZrO_2 doping on structure and superconducting properties of sintered DyBaCuO ceramics // Superconductor Science and Technology. 2001. Vol. 14, Is. 2, p. 59. https://doi.org/10.1088/0953-2048/14/2/301

19. Gorur O., Yildirim G., Altintas S.P., Terzioglu C. Role of Gd content in Cu(1) and Cu(2) sites on electrical, microstructural, physical, mechanical and superconducting properties of $YBa_2Cu_{3-x}Gd_xO_{7-\delta}$ ceramics // Journal of Materials Science: Materials in Electronics. 2013. Vol. 24, Is. 6, p 1842. https://doi.org/10.1007/s10854-012-1022-0

20. Rudnev I.A., Odintsov D.S., Kashurnikov V.A. Critical current suppression in high-T_c superconductors and its dependence on the defects concentration // Physics Letters A. 2008. Vol. 372, Is. 21, p. 3934. https://doi.org/10.1016/j.physleta.2008.02.065

21. MacManus-Driscoll J.L., Foltyn S.R., Jia Q.X., Wang H., Serquis A., Civale L., Maiorov B., Hawley M.E., Maley M.P., Peterson D.E. Strongly enhanced current densities in superconducting coated conductors of $YBa_2Cu_3O_{7-x}$ + $BaZrO_3$ // Nature Mater. 2004. Vol. 3. No.7, p.439. doi: 10.1038/nmat1156